Guidance and Control System Design of the Viking Planetary Lander

Robert N. Ingoldby*
Martin Marietta Aerospace, Denver, Colo.

This paper describes the salient features and unique problem solutions for the Viking lander guidance and control system design. Because of the following design requirements imposed, the lander guidance and control function presented stringent design challenges. These requirements were as follows: 1) a completely autonomous operation was required although the onboard computer memory size was limited to solve the descent problem; 2) the lander deorbit maneuver had to be very accurate to achieve a satisfactory planet atmospheric entry and an accurate touchdown at the predicted landing site; 3) the landers had to descend through an unknown atmosphere with a large variation in predicted characteristics, and they had to land at an unknown terrain height; and 4) they had to be as fuel-efficient as possible, particularly in the terminal descent phase. This paper describes how a safe and accurate landing on the surface of Mars while meeting these design requirements was achieved by the guidance and control systems of both Viking landers.

Introduction

THE guidance and control system design of the Viking lander will be discussed in two parts. First discussed will be the basic lander guidance and control problem and how the guidance and control subsystem was implemented to solve it, along with the unique design features of this implementation. Second, the actual lander performance as determined from use of flight telemetry data is presented along with comparisons to analytically determined predictions. Since most of the lander flight data are basically guidance and control oriented, these data will contain the essence of the lander's flight performance.

Design Approach and Unique Features

The Viking lander guidance and control system autonomously provides the navigation, guidance and control for the lander from separation of the lander from the orbiter to landing on the surface of Mars. Figure 1 (a pictorial review of the lander descent sequence) depicts the guidance and control problem.

The two Viking spacecraft, each consisting of an orbiter and a lander, orbitted Mars to acquire data for a precise landing, to enable the orbiter scientific instruments to determine whether the sites were suitable for landing, and whether surface moisture and temperature were compatible with the search for life. After suitable landing sites were selected, the landers received an onboard flight computer data update and electrical power turn-on signal. Preseparation checkout of critical descent equipment began about 30 h before separation.

Following separation, the lander was oriented for the deorbit maneuver by the reaction control system (RCS). The same RCS was then used to perform the deorbit. Following deorbit, the landers went into a relatively quiescent operational phase of attitude hold (called coast) until a predetermined time had elapsed, at which time the entry point (800,000 ft above the surface) was reached. This point was chosen as being safely above the Martian sensible atmosphere but still at least 7 to 10 min away from touchdown. At this point, the guidance and control system became very active again, the onboard flight computer came out of its low power "sleep" mode, and the lander was reoriented by the RCS to properly position the heat shield for Martian atmosphere encounter. At this time, the landers were traveling about 4.6 km/s (15,200 fps).

Velocity navigation was again started from bootstrap estimates of inertial velocity and position. The navigation process, except for attitude matrix integration, was stopped at the end of the deorbit phase to save power during the long coast phase. The bootstrap estimates of position and velocity were eventually corrected for any errors by subsequent updates, first from the radar altimeter which was turned on at 224 km (800,000 ft) for altitude updates, and then for velocity with respect to the surface updates from the terminal descent and landing velocity radar (TDLR) which was turned on during the parachute phase at approximately 4.57 km (15,000 ft) above the surface.

During entry, the aeroshell heatshield protected the lander from atmospheric heating by ablation. When the landers were about 5.79 km (19,000 ft) above the surface, the parachutes were deployed to slow the descent further. Seven seconds later the aeroshell was jettisoned, and 8 s later the landing legs were deployed. The parachute/base cover was jettisoned about 45 s later when the lander was 1.49 km (4900 ft) above the surface and descending at about 66 m/s (215 fps). Powered flight on the terminal descent propulsion system lasted about 40 s, with the three terminal descent engines being differentially throttled to control the lander pitch and yaw attitudes and also the lander velocity as a function of altitude. The terminal descent engines were shut down when the lander footpads contacted the Martian surface at about 2.44 m/s (8 fps). Honeycomb aluminum shock absorbers in the landing legs arrested the landers at touchdown. The nominal trajectory sequence is shown in Fig. 2.

The preceding design task was complicated because the functions were to be carried out automatically and completely autonomously. Two-way radio link transmission delay times were approximately 40 min, thereby precluding any meaningful Earth-based control once the initial separation signal was sent. Additionally, all design requirements were to be met while descending through any one of five postulated Martian atmospheres which varied in surface pressure from 4.99 to 9.3 mbars and landing at a surface elevation anywhere between +3.05 and −7.92 km (10,000 and 26,000 ft) with respect to mean surface level. The following sections will discuss the guidance and control functions in a task-oriented manner.

Presented as Paper 77-1060 at the AIAA 1977 Guidance and Control Conference, Hollywood, Fla., Aug. 8-10 1977; revision received Dec. 27, 1977.

Index categories: Entry Vehicles and Landers; Spacecraft Dynamics and Control; Spacecraft Navigation, Guidance, and Flight-Path Control.

*Senior Group Engineer.

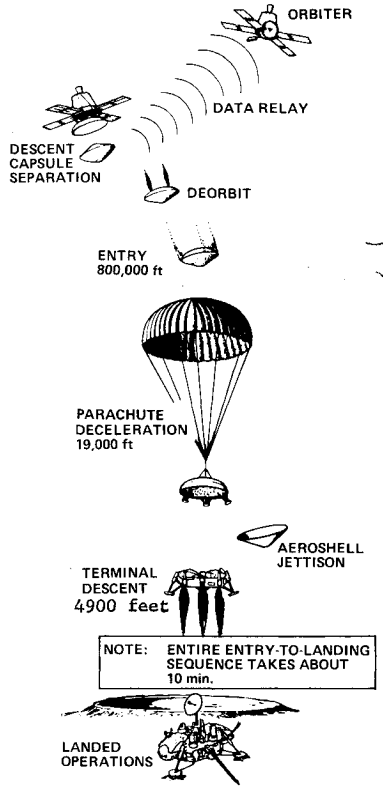

Fig. 1 Viking lander mission sequence.

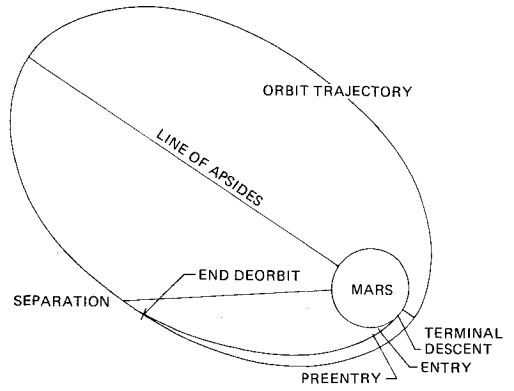

Fig. 2 Nominal *VL* descent trajectory.

Attitude Control

Except for the terminal descent phase, where the landers' pitch and yaw attitude were controlled by differentially throttling the terminal descent engines, all lander attitude control was handled by the attitude control system (ACS). The ACS is comprised of the attitude control logic equations, the inertial reference unit (IRU), and the RCS to implement the torque commands. The lander attitude is measured with respect to an inertial frame defined to be identity at lander separation by a first-order integration algorithm with orthonormality correction terms. The formulation for the second column of this attitude matrix $[A]$ is

$$\begin{bmatrix} A_{12} \\ A_{22} \\ A_{32} \end{bmatrix}_n = \begin{bmatrix} 1 & \Delta\theta_Z & -\Delta\theta_Y \\ -\Delta\theta_Z & 1 & \Delta\theta_X \\ \Delta\theta_Y & -\Delta\theta_X & 1 \end{bmatrix} \begin{bmatrix} A_{12} \\ A_{22} \\ A_{32} \end{bmatrix}_{n-1}$$

$$+E_{c2} \begin{bmatrix} A_{12} \\ A_{22} \\ A_{32} \end{bmatrix}_{n-1} - E_{c3} \begin{bmatrix} A_{13} \\ A_{23} \\ A_{33} \end{bmatrix}_{n-1} \tag{1}$$

where the $\Delta\theta$'s are the incremental angles of roll, pitch, and yaw obtained from the IRU rate integrating gyro rebalance pulse counts. E_{c2} and E_{c3} are the orthonormality correction coefficients necessary to maintain the A matrix axes orthogonal and normal because of the simple integration algorithm. They are defined by

$$E_{c2} = \tfrac{1}{2}[1 - (A_{12}^2 + A_{22}^2 + A_{32}^2)] \tag{2}$$

$$E_{c3} = \tfrac{1}{2}(A_{12}A_{13} + A_{22}A_{23} + A_{32}A_{33}) \tag{3}$$

The third column is computed similarly and the first column is obtained from the cross product of the previously computed elements.

The attitude matrix integration was carried out throughout the whole of the descent which lasted upwards of 6 h. The process is never updated with sensor measurements, so any error accrued in either the integration algorithm or the IRU gyro bias accumulation remains in the attitude matrix and affects the accuracy of subsequent maneuvers.

Computer simulations have shown that for this application, which had few fast maneuvers in the first part of the flight and a long quiescent coast time, the preceding formulation was able to meet the overall accuracy objectives. For the 24-bit computer word length and an update rate of 20 ms, the A matrix drift rate was less than 0.1 deg/h except during high-rate transients which occur late in the flight, primarily during the parachute phase.

Attitude maneuvers using the ACS are accomplished in the following manner. Given a desired attitude matrix for the lander to have $[A_d]$, an attitude error matrix $[\Delta A]$ can be formulated:

$$[\Delta A] = [A]\ [A_d]^T \tag{4}$$

where T denotes matrix transpose. Roll, pitch, and yaw errors are derived from the off-diagonal terms of ΔA:

$$\begin{aligned} \phi_e &= 0.5(A_{23} - A_{32}) \\ \theta_e &= 0.5(A_{31} - A_{13}) \\ \psi_e &= 0.5(A_{12} - A_{21}) \end{aligned} \tag{5}$$

This technique gives good roll, pitch, and yaw errors for small angle errors and at least gives the proper direction to turn in for larger errors. Certain singularity avoidance problems exist around 180 deg of error. Software logic is incorporated to avoid these problems by commanding a large command torque when the 180-deg singularity is sensed. The technique always commands a maneuver of less than 180 deg, and the maneuver can occur simultaneously about all three lander body axes, thus minimizing maneuver time. The lander can also be allowed to drift in an uncontrolled state as long as the true attitude matrix $[A]$ is computed. The lander will recover to the desired orientation $[A_d]$ when the attitude control loop is closed.

The foregoing attitude errors are fed into a standard attitude control phase plane switching logic which controls the operation of the eight aft pointing pitch/yaw RCS engines and four roll jets arranged in a butterfly configuration (see Fig. 3).

Deorbit

To save the weight of a separate high-thrust deorbit engine, the deorbit propulsive burn was accomplished with the eight, aft-pointing RCS engines. These engines are nominally low-thrust engines of 36 N (8 lbf) at a tank pressure of 240 N/cm^2 (348 psia). The burn time of the deorbit phase to accomplish a ΔV of 156 m/s is about 22 min.

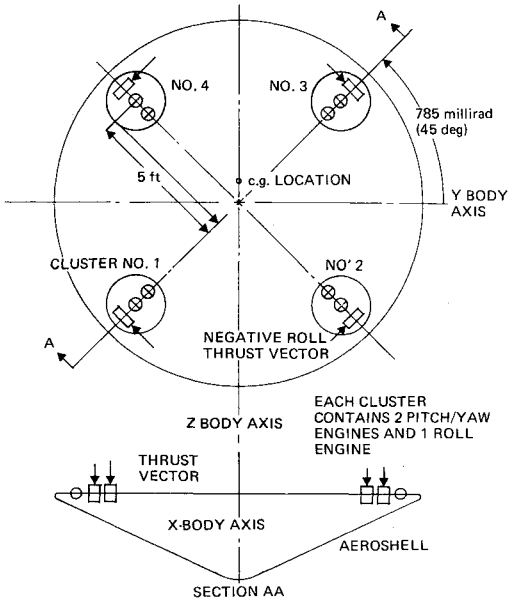

Fig. 3 Reaction control system geometry.

The accuracy of this burn is of prime importance in determining subsequent trajectory parameters such as entry velocity flight path angle and the coordinates of the touchdown point. Figure 4 shows the components of the landing ellipse semimajor axis predicted errors. The difference over the width of the bars depends on whether the deorbit is targeted to stay in plane (error to the left) or to cross range up to a maximum of 6 deg (error to the right). As can be seen, the maximum errors are caused by the deorbit execution. The orbit determination error is caused mostly by imprecision as to where the spacecraft is in its orbit rather than by what that orbit is. The entry systems' statistical errors are the result of an unknown magnitude and direction of atmospheric winds and uncertain aero-coefficient performance in the Martian atmosphere, since neither the aeroshell or parachute could be tested in the Martian atmosphere. Map and pole errors are simply imprecise knowledge of the targeted landing site on the surface of Mars to the known pole and map location.

The nonstatistical errors were assumed to come from the effects of the five unknown atmosphere models (discussed previously). They were treated as equally probable and in a nonstatistical manner. Finally, it was known that an accelerometer bias shift could occur if IRU heating by the deorbit engines occurred. Since the heating model was imprecise, it was decided to account for the worst-case heating. This then meant that the worst-case accelerometer bias shift was assumed to occur deterministically. As it turned out, little heating did actually occur, but at least the targeting accounted for the worst-case.

To minimize the errors associated with the deorbit burn, a velocity-to-be-gained guidance steering technique was used. Velocity-to-be-gained is the difference between the actual vehicle velocity accrued at any time and that value required to achieve the desired transfer trajectory. In body coordinates, these velocity-to-be-gained velocities are

$$\begin{bmatrix} V_{gxb} \\ V_{gyb} \\ V_{gzb} \end{bmatrix} = [A] \begin{bmatrix} V_r A_{d11} - V_{XI} \\ V_r A_{d12} - V_{YI} \\ V_r A_{d13} - V_{ZI} \end{bmatrix} \tag{6}$$

where V_r is the required velocity at any time defined from

$$V_r = C_0 + C_1 t + C_2 t^2 + C_3 t^3 + C_4 t^4 \tag{7}$$

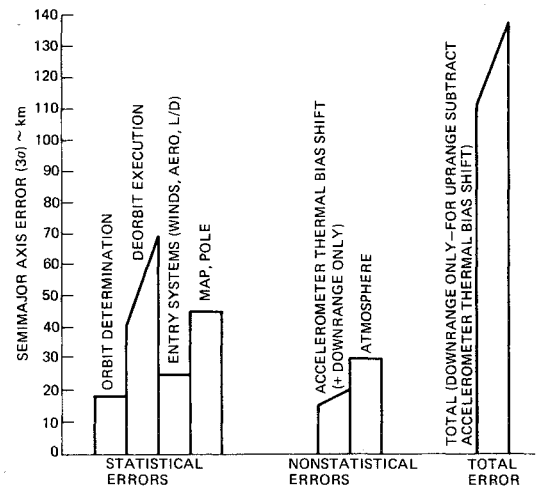

Fig. 4 Components of landing elipse semimajor axis errors.

and V_{XI}, V_{YI}, V_{ZI} are accrued inertial velocity changes from the start of the burn without gravity effects using the accelerometer integrated outputs over one integration time interval:

$$\begin{bmatrix} V_{XI} \\ V_{YI} \\ V_{ZI} \end{bmatrix}_n = \begin{bmatrix} V_{XI} \\ V_{YI} \\ V_{ZI} \end{bmatrix}_{n-1} + [A]^T \begin{bmatrix} V_{xb} \\ V_{yb} \\ V_{zb} \end{bmatrix}_n \tag{8}$$

and A_{d11}, etc, are elements of the desired body attitude matrix during the deorbit burn.

The steering laws using these velocities-to-be-gained in pitch and yaw are

$$\theta_c = \theta_{co} + GV_{gzb}$$
$$\psi_c = \psi_{co} - GV_{gyb} \tag{9}$$

where θ_{co} and ψ_{co} are accumulations of back value residuals in removing previous θ_c's and ψ_c's, and G is the velocity-to-be gained gain which, for best stability and error removal, was found to be 0.1.

This technique proved best able to account for thrust misalignments and attitude control limit cycle effects. It continuously keeps track of where the total velocity vector is being accrued in inertial space to the accuracy of measurement by accelerometers and the attitude matrix $[A]$ accuracy.

Since the burn time was close to ½ h and therefore very much *not* like an impulsive maneuver, errors in ΔV accumulation vs time and of cutoff time itself have a profound effect on subsequent trajectory parameters. This was the reason for the unique velocity-required function V_r. This function was sized to enable the vehicle to always be able to follow it even with an engine out and with degraded engine thrusts. This technique assured that the inertial velocity ΔV as a function of time and then, therefore, position was always close to that desired to within the thrust modulation technique used, i.e.,

$$V_{gxb} > V_{ed} \quad \text{turn all engines on} \tag{10a}$$
$$V_{gxb} < -V_{ed} \quad \text{turn all engines off} \tag{10b}$$
$$-V_{ed} \le V_{gxb} \le V_{ed} \quad \text{no change} \tag{10c}$$

where V_{ed} is an acceptable ΔV accumulation error of 0.305 m/s (1 fps).

These deorbit guidance techniques removed the effects of engine thrust misalignments, control system limit cycle ef-

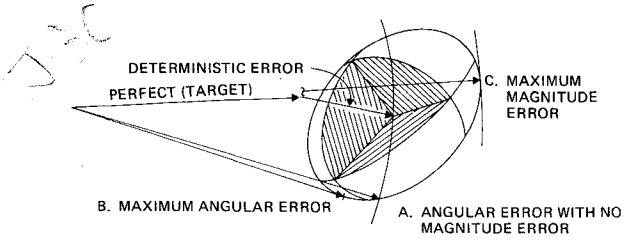

Fig. 5 Deorbit velocity increment dispersion.

fects, c.g. offset errors, engine I_{sp} errors, engine tank pressure errors, and engine thrust errors. Essentially the only remaining error contributors were those associated with how well we knew the vehicles' attitude through $[A]$ and how well we could measure the vehicles' acceleration by the accelerometers.

A comprehensive error analysis examining all error sources such as initial alignment of the spacecraft to the assumed celestial frame, gyro bias, gyro g sensitive drift, gyro g^2 sensitive drift, gyro scale factor, gyro misalignment, accelerometer bias, accelerometer scale factor, and accelerometer misalignment was done to assess the impact of these errors on the deorbit burn accuracy. These error sources each contribute to deorbit ΔV error with three inertial error velocity components that are correlated with each other. The root sum square of these components form the axes of a trivariate error elipsoid whose 99% probability surface is at the $3.4-\sigma$ level (see Fig. 5). Searching the surface of this $3.4-\sigma$ elipsoid for combinations of deorbit ΔV pointing and magnitude error produces the results shown in Fig. 6, which are well below the requirements. The deterministic error shown was due to the accelerometer bias that was not compensated for. The results shown are for the first Viking mission. The second mission results are very similar.

Of all the error sources mentioned, accelerometer bias along the thrust axis contributed nearly all of the error to deorbit ΔV magnitude, and lateral accelerometer bias plus the errors in initial alignment of the lander to the assumed celestial frame causes most of the error in deorbit ΔV pointing error.

Coast

As described in the mission description section, coast is a relatively quiescent phase, with attitude hold being the only ACS activity. The onboard flight computer is in a low-power "sleep" mode to conserve power, except for occasional "awake" times for attitude matrix integration, attitude control, and other necessary functions.

Entry

At a predetermined time from separation, the computer commands an entry maneuver using the ΔA technique previously described to align the aeroshell for atmosphere encounter. Entry navigation begins again, starting from predetermined velocity and position estimates. Soon after the entry point is reached, the sensible atmosphere is encountered and the attitude hold mode of control in pitch and yaw is released to the aeroshell dynamic stability control when 0.05 g is sensed. The ACS provided additional rate damping.

Also, at the time of entry navigation start, the attitude matrix $[A]$ reference frame is switched from the celestial reference obtained by the orbiter at separation to a reference frame coincident with an assumed touchdown frame at the assumed touchdown point (see Fig. 7). The reason for this is twofold: 1) it facilitates terminal descent navigation, and 2) it enables control to be obtained in the proper frame. For instance, it is necessary to keep the aeroshell lift vector in the vertical plane and to keep the radar altimeter antenna on the bottom of the aeroshell looking down. This is accomplished during the entry aeroshell phase by using A_{23} as a roll control

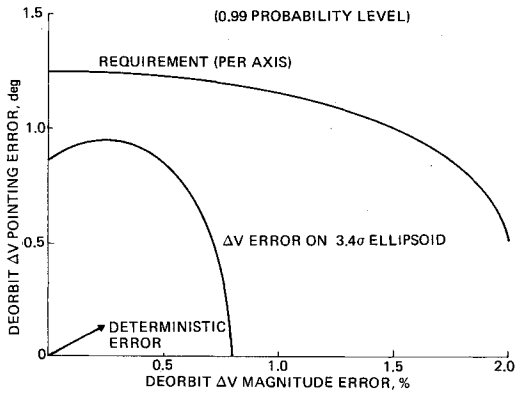

Fig. 6 Viking 1 deorbit ΔV error prediction vs requirement.

steering command. Nulling A_{23} keeps Y_{body} perpendicular to the down direction.

Parachute Phase

Attitude roll control and pitch and yaw rate damping are maintained during the initial part of the parachute phase. Early control system mechanizations then went to roll gyro attitude (body roll angle) hold at aeroshell drop to maintain the proper roll orientation on down to landing. Roll orientation of the lander at touchdown is important to assure that the proper sun angles are obtained for the camera imagery. Refinement of the parachute dynamic simulations late in the software test program (to incorporate a proper parachute lift vector) revealed a significant problem with roll gyro attitude hold. The parachute lift vector precessed around the vehicle roll axis producing a pseudoconing motion about the roll axis. Since we were holding *body* roll angle to zero, this roll axis coning motion induced a significant inertial roll error by the time the lander touched down. Figure 7 shows that the lander will land with its X axis coincident with the touchdown Z axis with some known roll angle ϕ orientation; so two ordered rotations about pitch θ and roll ϕ will transform from one frame to the other. The transformation from the touchdown frame to the desired frame is then

$$\begin{bmatrix} C\theta & 0 & -S\theta \\ S\phi S\theta & C\phi & C\theta S\phi \\ C\phi S\theta & -S\phi & C\theta C\phi \end{bmatrix} \tag{11}$$

The solution to this roll control problem, then, was to command a roll angle of

$$\phi_c = \phi_{cd} - \tan^{-1}\left(\frac{A_{32}}{A_{22}}\right) \tag{12}$$

where ϕ_{cd} is the desired roll orientation in the touchdown frame.

Note that, until the vehicle has completed its gravity turn profile to bring the vehicle X axis vertical, the vehicle A matrix will not necessarily approach Eq. (11). However, this is not a problem because the lander always completes nearly all of the gravity turn at a high enough altitude to assure that Eq. (12) will provide the proper roll steering before touchdown.

Terminal Descent

At approximately 1.49 km (4900 ft) above the surface, the terminal descent engines are started and warmed up. Two seconds later the parachute is released and the terminal descent control system pitch, yaw, and velocity control

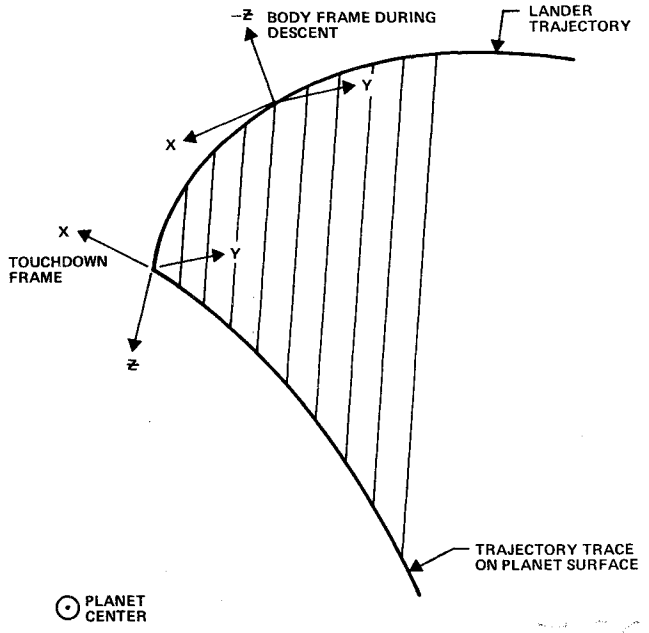

Fig. 7 Touchdown and body frames.

channels are closed (see Fig. 8). These control loops are closed through the digital computer where the steering, navigation, engine mixing, and digital compensation equations are implemented. The sampled-data stability margins for these digital control loops are shown in Fig. 9, along with the minimum margins under tolerance conditions.

Considerable linearization of these control loops, particularly of the gravity turn dynamics, was required for a linear analysis. References 1 and 2 present these linearization techniques. The validity of these techniques has been checked with an analog-hybrid 6-degree-of-freedom (DOF) nonlinear simulation of the terminal descent phase by breaking the loops at appropriate places and checking phase and gain. This has shown very good agreement.

It is instructive to review Fig. 8 with some detail. The two pitch and yaw steering commands are

$$\beta_c = G_\beta(\hat{v}/\hat{u}), \qquad \alpha_c = G_\alpha(\hat{w}/\hat{u}) \tag{13}$$

where G_β, G_α are steering gains. These are the gravity turn steering equations used to place the thrust vector opposite the total relative velocity vector to achieve a gravity turn trajectory.

The descent contour shown is altitude-velocity guidance. There were some unique problems associated with this guidance scheme that were also uncovered in the analytical simulation and performance test work.

Before delving into these problems, the basic terminal descent guidance problem will be discussed. Because of the variety of Martian atmospheres, winds, and terrain heights that the lander must contend with, there is a large range of initial velocity conditions at the end of the parachute. The velocity conditions range from

$$40\ \text{m/s} < V_V < 75\ \text{m/s} \tag{14a}$$

$$0\ \text{m/s} < |V_H| < 80\ \text{m/s} \tag{14b}$$

where V_V is the vertical velocity and V_H is the horizontal velocity with respect to the surface. Referring to the right-hand altitude velocity contour in Fig. 10, the initial technique of altitude-velocity guidance was to design a single H-V contour for a set of statistically determined worst-case initial velocities from the parachute phase. It was thought that any lesser velocity, no matter what its components, would be able to follow this "high-velocity" contour. As it turned out, for some combinations of velocity conditions the vehicle was not able to follow the contour and fell continuously behind it, eventually impacting on the surface at high velocity. The reason for this is obvious upon examination of the acceleration required to follow the H-V contour a_R:

$$a_R = \cos\psi\left[\frac{V\cos\alpha(1-\tan\psi\tan\alpha)}{f'(V)} + g\right] \tag{15}$$

where ψ, α are as shown on Fig. 11, V is the total vehicle

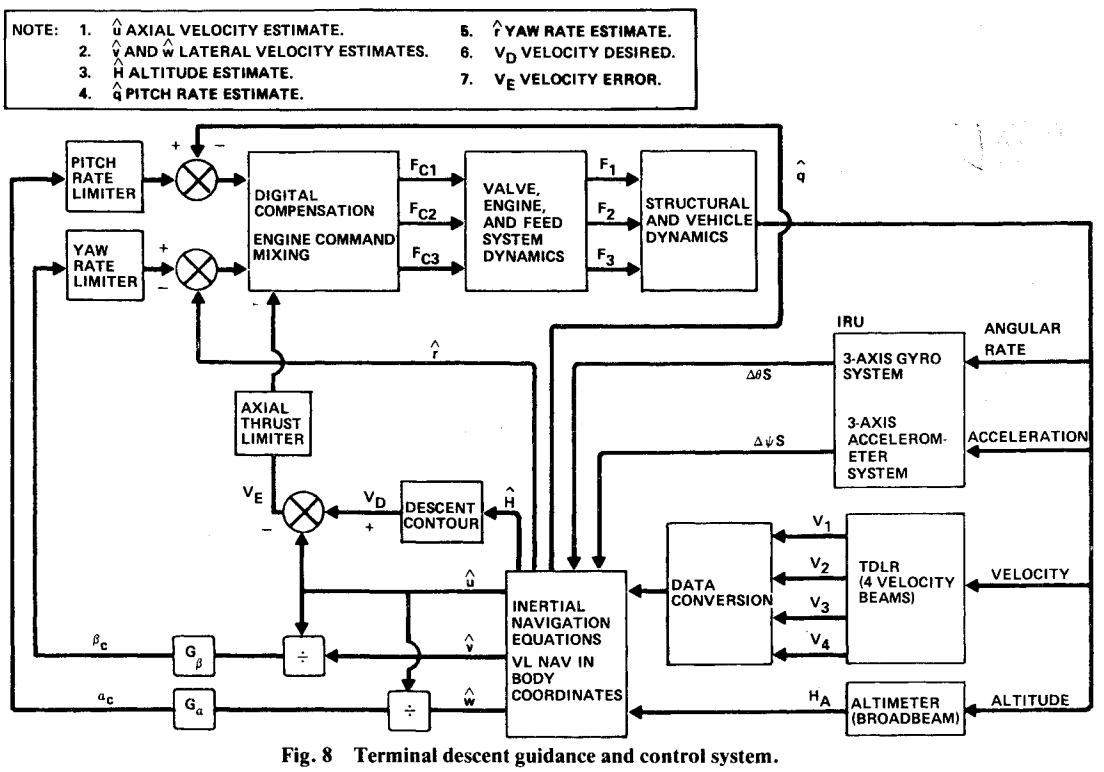

Fig. 8 Terminal descent guidance and control system.

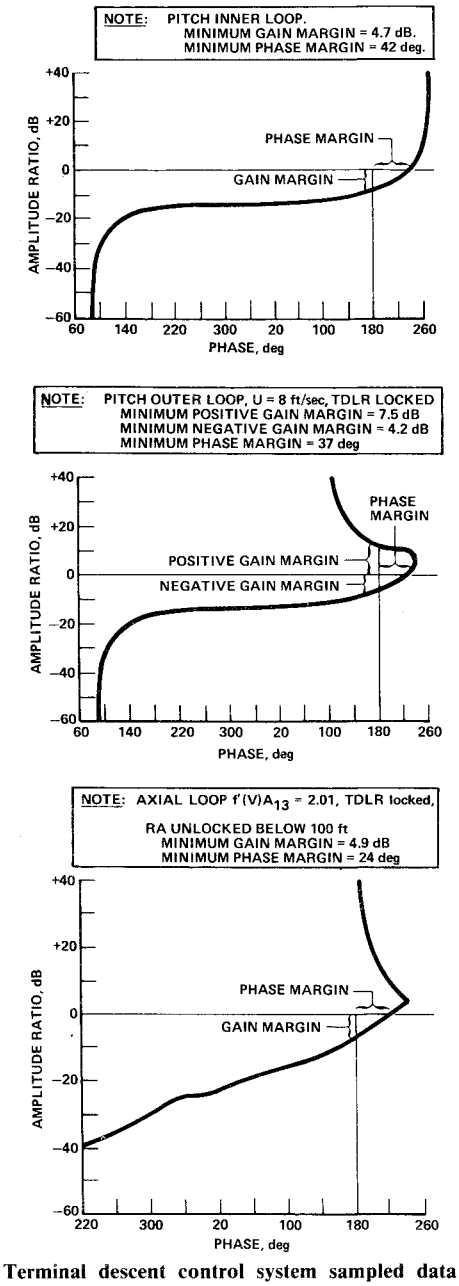

Fig. 9 Terminal descent control system sampled data open-loop frequency response.

relative velocity and

$$f'(V) = \frac{df(V)}{dV}$$

the slope of the contour function, $f(V) = H_d$.

For surface slope of zero, Eq. (15) becomes Eq. (16). Equation (16) shows the reason for the aforementioned problem. Along the design contour, a certain V-ψ combination exists at any altitude. Since our control law only worked with V, the total velocity, it was possible to intersect the contour with a ψ that was less than the design which could require an acceleration to follow the contour greater than the maximum available. This is what caused low-ψ, high-velocity cases to fall continuously behind the contour and impact at velocities greater than 8 fps. Other investigators have investigated other guidance techniques[3,4] such as range-velocity ($R-V$) guidance, altitude rate-altitude guidance ($\dot{H}-H$). These are fraught with the same types of problems, $R-V$ guidance being very sensitive to surface slopes and $\dot{H}-H$ guidance being sensitive to high ψ's.

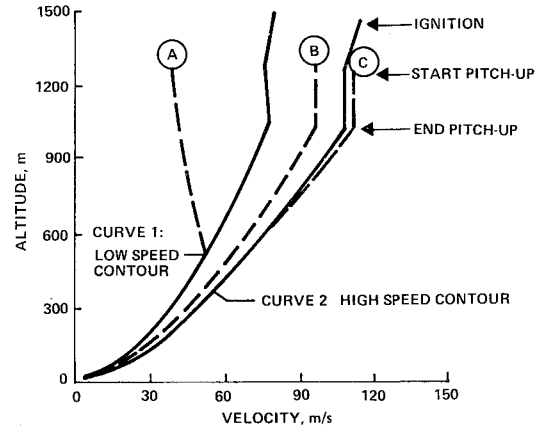

Fig. 10 Terminal descent altitude-velocity contours.

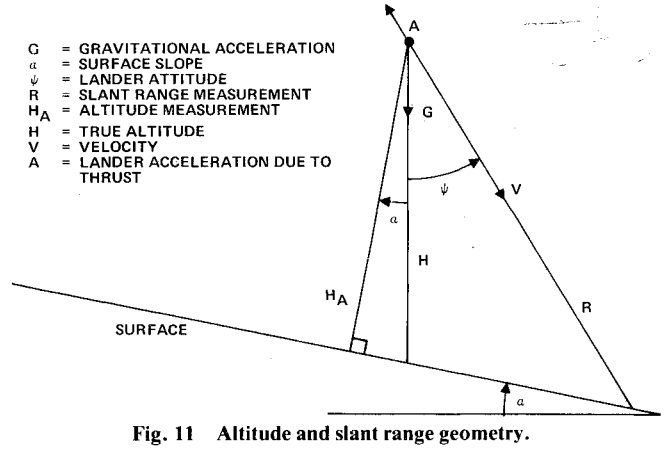

Fig. 11 Altitude and slant range geometry.

$$a_R = \cos\psi \frac{V}{f'(V)} + g \tag{16}$$

What was needed was some technique other than a basic guidance law change. Also, it was desirable to not use techniques such as an onboard real-time calculation of optimum descent contours given initial velocity conditions from the parachute. The flight computer capabilities for the descent program were severely limited in terms of both memory and timing. This was necessary because this computer had a multitude of additional functions besides descent to perform. The most important landed science and data handling functions are the prime users of the computer memory.

The dual-contour scheme shown in Fig. 10 was able to solve the foregoing problem with a minimum of computer impact. The right-hand contour is still designed to handle the maximum velocity conditions (as before with $H-V$ guidance) through a gravity turn. This gravity turn design contour is very nearly fuel-optimum for the initial design conditions. Thus, it is desirable not to have a guidance technique that departs from this to handle the highest velocity fuel-limiting case. Now, what causes ψ to decrease and for a_R to increase is for the horizontal velocity to decrease, so we can design a left-hand contour to the worst-thrust limiting case with $V_V = 75$ m/s, $V_H = 0$. Any initial velocity condition to the left of this left contour (see Fig. 10, condition A) is either purely vertical, $\psi = 0$ (for which the left contour was designed), or has some horizontal velocity, $\psi > 0$, which is a less severe thrust-to-weight condition. Initial velocity conditions between the two contours (see Fig. 10, condition B) are handled by a linearly interpolated contour between the two contours. The assumption here is that the only way we can be in this region is for the vertical velocity to be near the maximum value and the horizontal velocity has increased from zero. Initial conditions

Table 1 Touchdown error predictions

	Velocity in body axes, mps			Attitude rates, deg/s			Attitude errors, deg		
	Roll, U	Pitch, V	Yaw, W	Pitch, $\dot{\theta}$	Yaw, $\dot{\psi}$	Roll, $\dot{\phi}$	Pitch, θ	Yaw, ψ	Roll, ϕ
Viking 1	2.44 ± 0.44	0 ± 0.35	0 ± 0.53	0 ± 0.65	0 ± 1.08	0 ± 1	0 ± 0.65	0 ± 1.08	$\phi_{co} \pm 10$
Viking 2	2.44 ± 0.37	0 ± 0.22	0 ± 0.43	0 ± 0.85	0 ± 1.08	0 ± 1	0 ± 0.85	0 ± 1.08	$\phi_{co} \pm 10$
Requirement	2.44 ± 0.91	0 ± 1.22	0 ± 1.22	0 ± 7	0 ± 7	0 ± 3	0 ± 5	1 ± 5	$\phi_{co} \pm 10$

Table 2 Estimated deorbit errors

	Pointing, deg (σ)	Magnitude, % (σ)	Touchdown error, km (σ)
Viking 1	0.24(0.84)	0.20(1.27)	−24(1.06)
Viking 2	0.29(1.01)	0.055(0.35)	+9.0(0.40)

to the right of contour 2 (Fig. 10, condition C) were never meant to be designed to, but if they are encountered, the right-hand contour is used. If they are not too high in velocity, then the fuel and throttle margins provided in the terminal descent system would enable the lander to "catch up" to the right-hand contour, as shown, and land successfully. Performance test and simulation work done on a multitude of initial velocity conditions has shown that all initial velocity conditions within the initial design velocity bounds ($V_V \leq 75$ m/s, $V_H \leq 80$ m/s) were able to be handled.

Touchdown

The touchdown conditions of lander velocity, attitude, and attitude rate are the most important elements of the entire descent sequence for which all other elements of lander performance are predecessors. Error analyses have been performed for these touchdown conditions considering the effects of velocity radar noise and biases, inertial sensor and attitude matrix misalignment and biases, wind forces, and engine misalignment and thrust noise. Table 1 presents the results of this analysis, and shows the nominal value expected plus the 99% tolerance value. The values shown on the bottom line are the system requirement values imposed on the system to insure a successful landing.

Performance Achieved

Both Viking landers successfully landed on the surface of Mars. The descent performance of each lander was virtually nominal with very little error. The following sections discuss the descent performance, which was obtained primarily from Ref. 5.

Deorbit

Separation, the maneuver for deorbit and deorbit itself, went very smoothly and nominally for both landers. The deorbit burns ended within 2.8 s of the predicted time for lander 1 and 0.1 s for lander 2. A time difference up to 6 was acceptable.

Although no direct measurements of lander velocity and position are available, it is possible to reconstruct the trajectory by using the lander gyro and accelerometer data telemetered back to Earth. Using these estimates, the estimated deorbit execution errors were obtained (see Table 2). The σ levels shown relate to the error analysis predictions.

Table 4 Altitude errors at parachute deployment and terminal descent ignition

	Viking 1, m	Viking 2, m	Maximum allowable, m
Parachute deployment	83	68	±168
Engine start	1	2	±91

Entry Conditions

The deorbit errors described earlier and the orbit determination errors translate into velocity and position errors at the entry point, shown on Table 3. These numbers are in excellent agreement to the targeted values. The onboard navigator performance is strongly dependent on these initial condition errors. All errors shown are significantly less than what the guidance and control subsystem is capable of handling. It resulted in subsequent small errors in parachute deployment and engine ignition altitude shown in Table 4.

In fact, most of the parachute deployment errors resulted from not having a radar altimeter bias error of 46 m which was planned on but nonexistent because of the very strong radar signal return. The errors were well within acceptable tolerances.

Terminal Descent

The terminal descent phase was very close to nominal. Engine valve position received from telemetry data looked much like simulation data. Fuel usage was 68.66 kg for lander 1 and 68.70 kg for lander 2 (total was 83.91 kg).

The last phase of the contour was a constant velocity phase which was supposed to last for 16.8 m. However, it lasted for about 19.2 m for both landers. This error was eventually traced to a radar altimeter bias error on both landers resulting from an altimeter calibration error just before launch.

Table 3 Entry velocity conditions

	Viking 1			Viking 2		
	Target	Estimate	Error, σ	Target	Estimate	Error, σ
Inertial vel, km/s	4.61000	4.60989	0.01	4.61430	4.61216	0.23
Inertial flight path angle, deg	−16.900	−16.995	0.34	−17.005	−17.084	0.25
Lat-aerocentric, deg	12.575	12.503	0.20	36.586	36.476	0.22
Long, deg	62.004 west	62.151 west	0.28	243.036 west	243.131 west	0.15

Table 5 Touchdown conditions

	Velocity, m			Attitude rates, deg/s			Attitude error, deg		
	U	*V*	*W*	Roll	Pitch	Yaw	Roll	Pitch	Yaw
Viking 1	2.49	−0.01	−0.16	0.48	−0.92	−0.41	1.63	0.59	0.34
Viking 2	2.47	−0.03	−0.20	−0.12	−1.23	1.94	0.92	−1.16	−2.18
Desired	2.44	0±1.22	0±1.22	0±5	0±7	0±7	0±10	0±5	0±5

However, this small error was not significant, since it resulted in using only 1 kg additional fuel of the fuel margin provided.

The touchdown conditions achieved for both landers are shown in Table 5. These final touchdown results exemplify all of the other results achieved by the guidance and control subsystems of both Viking landers. The performance was almost completely nominal and the errors experienced were well within the statistical errors predicted.

Acknowledgment

The excellent performance achieved by both Viking landers has provided another milestone in the development of planetary lander guidance and control systems. This performance is a tribute to the years of design analysis, simulation, and performance testing done on the Viking lander and paraticularly a tribute to the many review cycles and helpful critiques by NASA.

References

[1] Stafford, P.S. and Ingoldby, R.N., "Guidance and Control Design for A Six-Engine Martian Soft Lander," AAS/AIAA paper 68-6-3, *Space Projections from the Rocky Mountain Region,* July 15-16, 1968.

[2] Ingoldby, R.N., "Terminal Descent Phase Digital Control System Analysis," Martin Marietta Corporation, Denver, Colo., TN-3T10038, June 1970.

[3] Stafford, P.S., "A Quantitative Comparison of Altitude–Velocity and Range–Velocity Guidance for Terminal Descent," Martin Marietta Corporation, Denver, Colo., TN-3770113, July 30, 1971.

[4] Cheng, R.K., "Terminal Guidance for a Mars Soft Lander," *Eighth International Symposium on Space Technology and Science,* Tokyo, Japan, 1969.

[5] Ingoldby, R.N., et al., "Entry Analysis for Viking Landers 1 and 2," Martin Marietta Corporation, Denver, Colo., TN-3770218, Nov. 1976.